Is that a relict rock glacier?

Colucci, Renato R.; Forte, Emanuele; Žebre, Manja; Maset, Eleonora; Zanettini, Carlotta; Guglielmin, Mauro

Published in:
Geomorphology

DOI:
10.1016/j.geomorph.2019.02.002

Publication date:
2019

Citation for published version (APA):
Colucci, R. R., Forte, E., Žebre, M., Maset, E., Zanettini, C., & Guglielmin, M. (2019). Is that a relict rock glacier? *Geomorphology*, *330*, 177-189. https://doi.org/10.1016/j.geomorph.2019.02.002

Is that a relict rock glacier?

Renato R. Colucci*[,a], Emanuele Forte[b], Manja Žebre[c], Eleonora Maset[d,e], Carlotta Zanettini[b], Mauro Guglielmin[f]

a. Department of Earth System Sciences and Environmental Technology, ISMAR-CNR Area Science Park Basovizza, Q Building, S.S.14 km 163.5, I-34149, Trieste-Italy

b. Department of Mathematics and Geosciences, University of Trieste, via Weiss 2, Trieste-Italy

c. Department of Geography & Earth Sciences, Aberystwyth University, Llandinam Building, Penglais Campus, SY23 3DB, Aberystwyth, United Kingdom

d. Helica s.r.l., Amaro (Udine), Italy

e. Polytechnic Department of Engineering and Architecture, University of Udine, via Palladio 8, 33100 Udine, Italy

f. Department of Theoretical and Applied Sciences Insubria University, via J.H. Dunant, 21100 Varese, Italy

*corresponding author. E-mail address: r.colucci@ts.ismar.cnr.it (R.R. Colucci)

Keywords: rock glacier, periglacial environment, buried ice, permafrost, Electrical Resistivity Tomography

Abstract

The distribution of rock glaciers is often used to investigate the occurrence of permafrost in mountain areas and to understand their climate and paleoclimate evolution. This requires the creation of regional and global inventories capable of discriminating active and relict landforms in order to forecast the presence or absence of ice in the ground. In this paper, geomorphological, geophysical and microclimatic surveys are

performed on a rock glacier of the Carnic Alps (Eastern European Alps). In the classification currently used for implementing regional inventories of permafrost evidence in the Alps, this rock glacier would be defined as relict. However the geophysical, climatological and geomorphological results indicate that internal iceis widespread in large portions of the rock glacier. These are generally interpreted as ice in pore spaces and local ice lenses, probably without layers of massive ice. Moreover the occurrence of ice during the maximum thawing season at depths < 15 m, assumed here as the depth of zero annual amplitude, suggests that the ice occurring within the rock glacier is related to current cryotic conditions due to density driven air flow (i.e. the chimney effect). This research demonstrates that the current altitudinal limit of alpine permafrost can be locally several hundreds of meters lower than forecasted by empirical modeling based only on the rock glacier distribution and classification. Therefore, rock glacier classifications based only on remote sensing and geomorphological evidence as the main sources for extracting regional climate and paleoclimate signals should be treated with caution.

1. Introduction

The term rock glacier defines a thick lobate or tongue-shaped mass of debris moving downslope through the deformation of subsurface ice and/or ice-rich sediments (Ballantyne, 2018). Generally, the downslope movement is indicated geomorphologically by a system of transverse surface ridges and furrows (Capps, 1910; Wahrhaftig and Cox, 1959). Although they are commonly present in many poorly-glacierized mountain regions around the world, rock glaciers represent key features for the understanding of high altitude cryosphere under climate change conditions (Haeberli et al., 2006). A long-running discussion exists around the origin of rock glaciers (Anderson et al., 2018). The ice within a rock glacier might come from ice-supersaturated mountain permafrost (e.g., Haeberli, 1985; Barsch, 1996), from glacier ice (e.g., Whalley and Martin, 1992, Guglielmin et al., 2018) or represents a continuum between glacial and non-glacial origin (e.g., Giardino et al., 1987; Clark et al., 1998; Humlum, 1998, 2000; Berthling, 2011;),
A common characteristic of rock glaciers is the presence of old buried ice, often (but not exclusively) of glacial origin (e.g., Guglielmin et al., 2004; Stenni et al., 2007; Ribolini et al., 2010;) and of different ages

(e.g., Krainer et al., 2015). It has been recently shown that presently active rock glaciers probably underwent long periods of inactivity in response to climate variability (i.e. warming) during the Holocene, although warmer periods produced only limited ice melt (Krainer et al., 2015). Thus, while glaciers are considered excellent climate indicators and their evolution is recognized as someof the best evidence for climate change (e.g., Haeberli et al., 2007), rock glaciers are generally more resilient to atmospheric changes due to their thick debris cover (Jones et al., 2018). In this context, it is important to discriminate between different rock glacier's evolutionary stages, and classify them accordingly. The rock glacier classification is generally performed by looking at their degree of activity, defining them as intact (active and inactive) and relict, and following different classifications proposed by Haeberli (1985), Barsch (1996) and Cremonese et al. (2011), all based on their dynamics. Active rock glaciers are characterized by widespread presence of buried ice, sufficient to induce internal deformation, creep and movement. Inactive rock glaciers also contain ice, but are no longer mobile either due to the melting of most of the upper ice layers within the terminus slope (climatically inactive), or because of topographic obstacles (dynamically inactive). Relict rock glaciersdo not flow and internal ice is assumed to be completely absent. Moreover, an additional type of rock glaciers, called pseudo-relict, has also been recognized and defined as an intermediate type between relict and inactive rock glacier, having locally isolated patches of permafrost (Barsch, 1996; Kellerer-Pirklbauer, 2008; Kellerer-Pirklbauer et al., 2012) with negligible climatic significance.

Ice distribution within rock glaciers varies considerably. Volumetric ice content within rock glaciers normally ranges between 40% and 60% (Barsch, 1996; Haeberli et al., 1998; Hausmann et al., 2007) although estimates of up to 70% have also been reported (Barsch et al., 1979; Arenson, 2002;). Considerable uncertainties remain regarding the ice content and subsequent water equivalent of inactive and pseudo-relict rock glaciers.

One of the peculiar characteristics of a rock glacier is to retain much of its original morphology, even after it has ceased moving and the internal ice has completely melted. Rock glaciers at this stage display less pronounced furrows and gentler front slopes compared to the same landform that was once active (Hughes et al., 2003). For this reason, rock glaciers can be mapped relatively easily from aerial photographs, and

76 further geometrically constrained and classified with more sophisticated digital elevation models (DEM),
77 obtained from high resolution aerial laser scanning or photogrammetric techniques. These methods are
78 widely used in compiling regional inventories, which often discriminate between intact and relict forms,
79 although generally without any geophysical or direct investigation. Such classifications are further used to
80 make estimations of permafrost presence (e.g., Scotti et al., 2013) and water volume equivalent (Jones et
81 al., 2018). One of the main indicators used in remote sensing to classify a rock glacier as *relict,* thus
82 excluding the occurrence of ice and movement, is considered to be the presence of (widespread)
83 vegetation cover (e.g.,; Seppi et al., 2005;; Scapozza and Mari, 2010; Lilleøren and Etzelmüller, 2011; Scotti
84 et al., 2013; http://www.permanetalpinespace.eu/archive/pdf/WP5_3_final_report.pdf; last accessed 4
85 July 2018) although it is well known that alpine vegetation can cover surfaces with displacement up to 35
86 cm/year (i.e. Cannone and Gerdol, 2003). Once classified, the altitudinal distribution of rock glaciers is often
87 used as a proxy for inferring permafrost occurrence and to extract climate and paleoclimate signals. A
88 correct interpretation of all these aspects is particularly important in areas of sporadic permafrost, as, e.g.,
89 the case of the Mediterranean mountains (Oliva et al., 2018). Here, it is still not clear which landforms flow
90 and/or contain ice, and what is the timing of their formation and stabilization (e.g., Hughes, 2018; Oliva et
91 al., 2018).
92
93 Geophysical techniques have been extensively used to investigate the internal structure of rock glaciers.
94 These include seismic (e.g., Musil et al., 2002), ground penetrating radar (GPR) (e.g., Arcone et al., 1998;;
95 Musil et al., 2006; Monnier et al., 2008; Merz et al., 2015; Guglielmin et al., 2018) and electrical (e.g.,
96 Kneisel and Hauck, 2008) methods. Such techniques are often integrated (Hausmann et al., 2007; Leopold
97 et al., 2011) and calibrated with boreholes and temperature measurements. As far as electrical methods
98 are concerned, the technical improvements of the last decades have provided increasingly accurate results.
99 Vertical resistivity soundings (VES) have been extensively used since the 1970's to investigate the internal
100 structure of rock glaciers (King et al., 1987; Guglielmin et al., 1994, 1997;). More recently, the development
101 of modern multichannel systems that can be connected to several tens of electrodes has allowed the
102 successful application of 2D electrical resistivity tomography (ERT) (e.g., Hauck et al., 2003; Hauck and

Mühll, 2003; Ribolini et al., 2010) as well as pseudo-3D ERT surveys (Rödder and Kneisel, 2012; Emmert and Kneisel, 2017;). The most significant problem in geoelectrical surveying on rock glaciers is the weak galvanic coupling associated with the generally high contact resistances between electrodes and ground (Maurer and Hauck, 2007), and the usually very rough topography, characterized by different size sediments and blocks. However, ERT investigations remain the most accurate geophysical techniques to distinguish between frozen and unfrozen areas (e.g., Hausmann et al., 2007; Hauck et al., 2011), even if there are uncertainties related to the resistivity range superposition between different geological and glaciological conditions (Reynolds, 2011). A comprehensive review of the pros and cons of geophysical techniques for rock glaciers imaging is provided by Maurer and Hauck (2007).

Rock glaciers on the southern side of the European Alps have been thoroughly studied using different approaches (Oliva et al., 2018) and the distribution of rock glaciers in the southeastern Alps has been recently updated by Colucci et al. (2016). Here, the altitudinal range of rock glaciers was found to be the lowest for the southern Alps, while the majority of rock glaciers were classified as relict. The Razzo rock glacier (RRG) in the Italian Carnic Alps is an example of a rock glacier that shows characteristics of a relict landform based only on its geomorphic properties, elevation range and vegetation cover. This work aims to: 1) describe the internal characteristics of a geomorphologically relict rock glacier through ERT investigations, repeated high resolution LiDAR surveys, and a three-year-long period of ground temperature monitoring; 2) discuss, with evidence from the RRG case study, the limitations of the present classifications when taking into account only geomorphic characteristics and vegetation cover in the implementation of regional inventories.

1. Study area

The RRG (Lat. 46°28’16.19” N; Long. 12°36’34.61” E) is located in the Italian Carnic Alps (Fig. 1). The highest peak of the study area is Mt. Tiarfin (2,413 m asl; Fig. 3), while the highest peak in the Carnic Alps is Mt. Coglians (2,782 m asl; Fig. 1b). The Tiarfin group is characterized by Triassic dolomitic limestone (*i.e. calcari dolomitici of Tiarfin*) in the highest parts, overlaying Permian Bellerophon, Val Gardena Sandstone and

Sesto Conglomerate towards the North (Carulli, 2006). Several rock glaciers and other landforms of periglacial origin have been described in inventoriees of the surrounding mountains (Colucci et al., 2016), while glaciers and ice patches are scattered and have only been reported from the Dolomites to the west (Baroni et al., 2017), in the area of Mt. Coglians (Carnic Alps) to the northeast (Colucci and Guglielmin, 2015) and in the Julian Alps to the east (Colucci and Žebre, 2016).

A useful source of climate information for the study area is the meteorological station of Mt. Zoncolan (1750 m) located 25 km east and at the same elevation as RRG. Here, the 1993-2017 Mean Annual Air Temperature (MAAT) was 4.2°C (σ=0.7) with February being the coldest month (-3.5°C, σ=2.5) and August being the warmest month (12.6°C, σ=1.8) (www.meteo.fvg.it; last accessed on 4 July 2018). 1993-2013 Mean Annual Precipitation (MAP) was 1,795 mm water equivalent (w.e.) with February being the driest month (36 mm w.e.) and November being the wettest month (255 mm w.e.).

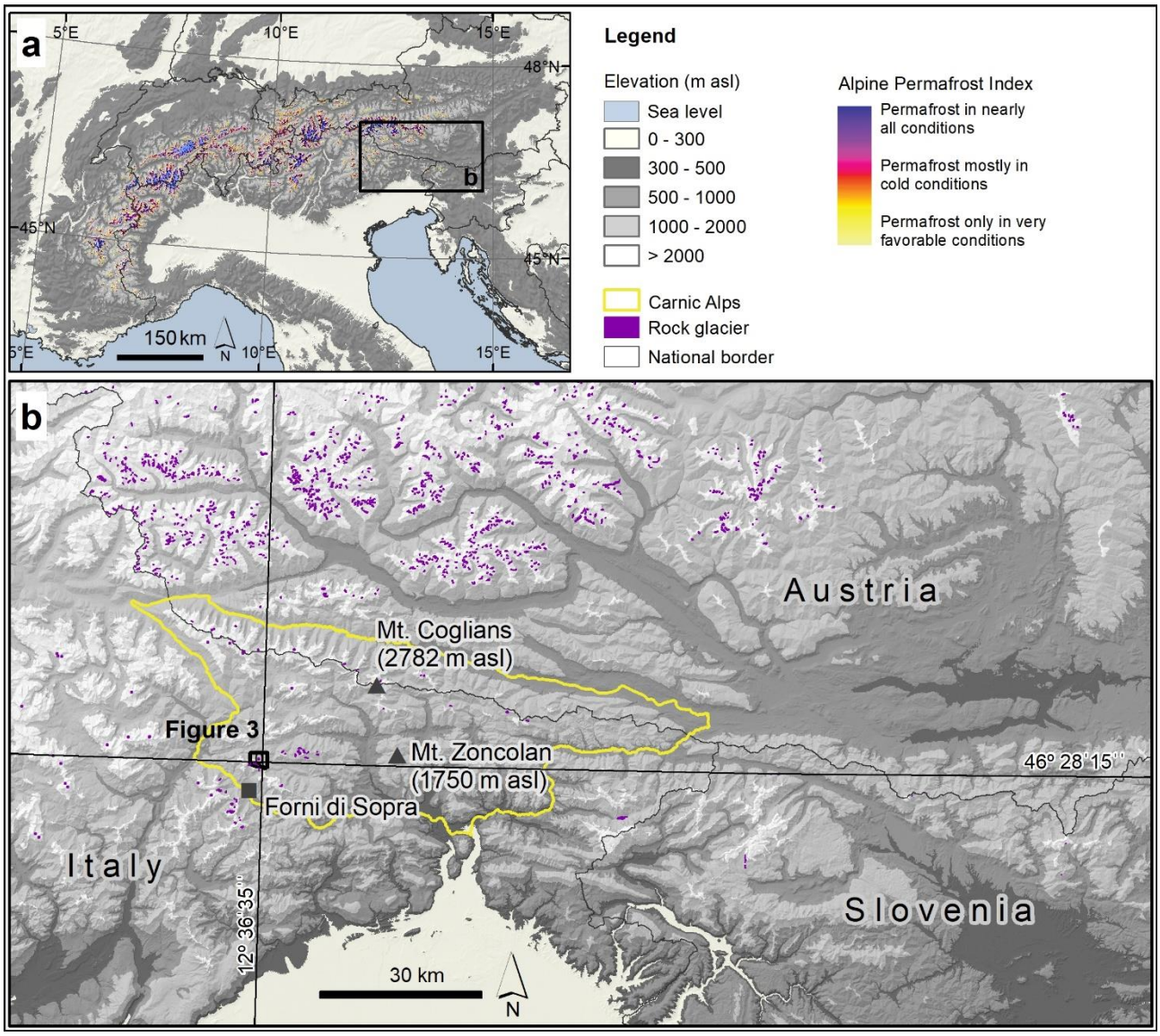

Fig. 1

(a) Permafrost distribution in the Alps according to the Alpine permafrost index map (Boeckli et al., 2012). (b) Rock glacier distribution in the southeastern Alps, including Central and Eastern Austria (after Lieb et al., 2012), Slovenia (after Colucci et al., 2016) and Italian regions of Friuli Venezia Giulia (after Colucci et al., 2016) and Veneto (after PermaNet; http://www.permanetalpinespace.eu/archive/pdf/WP5_3_final_report.pdf; last accessed on 4 July 2018). The latter inventory was performed using lower resolution DEM with respect to Lieb et al. (2012) and Colucci et al. (2016) and therefore probably underestimates the real number of landforms. The Razzo study area is located within the marked black square and reported in detail in Fig. 3.

2. Methods

3.1 LiDAR data acquisition and processing

Two airborne Light Detection and Ranging (LiDAR) surveys were carried out over the study area on August 2009 and September 2016, with an average point density of 4 and 8 points per square meter, respectively. Technical specifications of both surveys are reported in Table 1.

	2009 survey	2016 survey
Average flight height	800 m a.g.l.	1000 m a.g.l.
LiDAR system	Optech ALTM Gemini	Riegl LMS-Q780
Laser frequency	33 – 167 kHz	0 – 400 kHz
Acquisition mode	Up to 4 range measurements	Full-waveform
Scan angle	50°	60°
Average point density	4 points m^{-2}	8 points m^{-2}
Vertical accuracy	0.05 m at 250 m range	0.02 m at 250 m range
Horizontal accuracy	0.05 m at 250 m range	0.02 m at 250 m range

Table 1. Technical specifications of the two LiDAR surveys performed in the study area in 2009 and 2016.

A visual inspection of the two datasets showed a residual shift between them, which could affect subsequent analyses and generate misleading results in terms of surface changes. For this reason, the Iterative Closest Point (ICP) algorithm (Zhang, 1994) of the CloudCompare software was used to automatically co-register the two point clouds, adopting as a reference the point cloud from 2016. In particular, the ICP algorithm was applied on a subset of the point clouds, corresponding to stable (i.e. no surface change) areas, and the obtained rigid transformation was then applied to the whole original point cloud surveyed in 2009.

In order to create a representative model of the actual terrain surface excluding vegetation, a classification of both point clouds was carried out. First, the routines provided by TerraScan software package were used to generate an automatic classification. This classification was subsequently manually edited to accurately rearrange the datasets into two classes, namely ground points, i.e. points belonging to the terrain surface, and overground points, i.e. points backscattered by trees, shrubs, buildings and any other element above the terrain. Ground points were then exploited to create Digital Terrain Models (DTMs) with a resolution of 1 m. TerraScan software uses LiDAR points to derive a Triangulated Irregular Network (TIN) through Delaunay triangulation that is subsequently resampled onto a grid of specified resolution.

Finally, to highlight vertical elevation differences and the horizontal shifts of the study area, a DEM of Difference (DoD) was computed by subtracting the 2009 surface from the 2016 surface using the ESRI ArcGIS® raster calculator tool. The elevation difference error, computed on stable areas, is on average -0.06 m, with a standard deviation of 0.28 m.

3.2 Geomorphic Changes and Analysis

In order to identify and investigate possible geomorphic changes in the study area , vertical elevation differences between the DTMs derived from the 2009 and 2016 LiDAR point clouds were analyzed. To produce reliable results, uncertainties affecting DTMs and the obtained DoD were first taken into account. Several factors can indeed introduce errors in DTMs, including survey point quality, surface characteristics, sampling strategy, interpolation methods and classification errors (Milan et al., 2011).

In this study, we assumed spatially uniform uncertainties affecting the DoD and specified a threshold for the minimum level of detection to distinguish between actual surface changes and inherent noise. A threshold of 0.56 m was chosen, which corresponds to twice the standard deviation of the elevation difference error computed on stable areas, as described in section 3.1. In this way, predicted elevation changes beneath this detection limit were discarded. The thresholded DoD was generated using the ESRI ArcGIS Geomorphic Change Detection (GCD) tool (Wheaton et al., 2010).

189 Further statistical analysis was then performed with the GCD tool on the thresholded DoD and the results
190 are reported in Table 2.

191 *3.3 Geomorphological setting, rock glacier volume and water volume equivalent*

192 Although the focus of this research is the study of one particular rock glacier, we mapped the
193 geomorphology of a wider area, approximately equal to 6 km^2. Moraine and rock glacier ridges were
194 mapped using orthophotos and digital elevation models (DEM) derived from 2009 and 2016 LiDAR data
195 (Table 1), as well as field surveying. A detailed geomorphological analysis, including the calculation of some
196 typical rock glacier morphometric parameters (maximum, minimum and mean altitude, width, length, area,
197 mean slope of the front), was performed by applying different ESRI ArcGIS® tools.

198 The maximum volume of ice during full rock glacier activity in the past of the RRG was estimated on the
199 basis of assumed volumetric ice content (40-60 %) within intact rock glaciers and rock glaciers volume.
200 Volume of the RRG was estimated by multiplying rock glacier surface area (A) and thickness (H). The first
201 parameter was extracted from a 1 m DEM, using the previously defined rock glacier polygon. The second
202 parameter was estimated using an empirical rule established by Brenning (2005), which is based on several
203 field observations of rock glacier geometry. According to this power-law relationship (Equation 1) the mean
204 rock glacier thickness (H; in meters) is calculated as a function of surface area (A; in square kilometres) and
205 two scaling parameters (c and β)

206 $$H = cA^{\beta} \quad (1)$$

207 where c is 50 and β is 0.2.

208 The estimated ice volume was subsequently used for the calculation of the water volume equivalent
209 (w.v.e.) (Brenning, 2005; Jones et al., 2018) by assuming an ice density conversion factor of 900 kg m^{-3}
210 (Paterson, 1994).

211

212 *3.4 Ground temperature monitoring*

Ground temperature is measured at 2 different locations at the rock glacier's front by using Tynitag-plus-2® dataloggers, equipped with a built-in sensor and with thermistor probes with an accuracy of 0.35°C and a resolution of 0.01°C. The probes are located at the entrance of two decimetric-in-size natural cavities near the foot of the rock glacier's front, through which evident cold-air flow is detected in summer. Ground surface temperature (GST) at location 1 (Fig. 2a) is recorded by the built-in sensor at the ground surface and the datalogger is inserted into the ground with its top part at ground level, whilst ground temperature (GT-1) is recorded by a thermistor probe inserted 20 cm in the soil at the bottom of the small cavity, overall at 100 cm depth. Ground temperature (GT-2) at location 2 (Fig. 2b) is recorded in the same way as at location 1, whilst air flow temperature (ATH) is recorded by a thermistor probe vertically fixed in the small cavity. At both locations, the dataloggers are set to record the minimum and maximum temperature on a hourly basis.

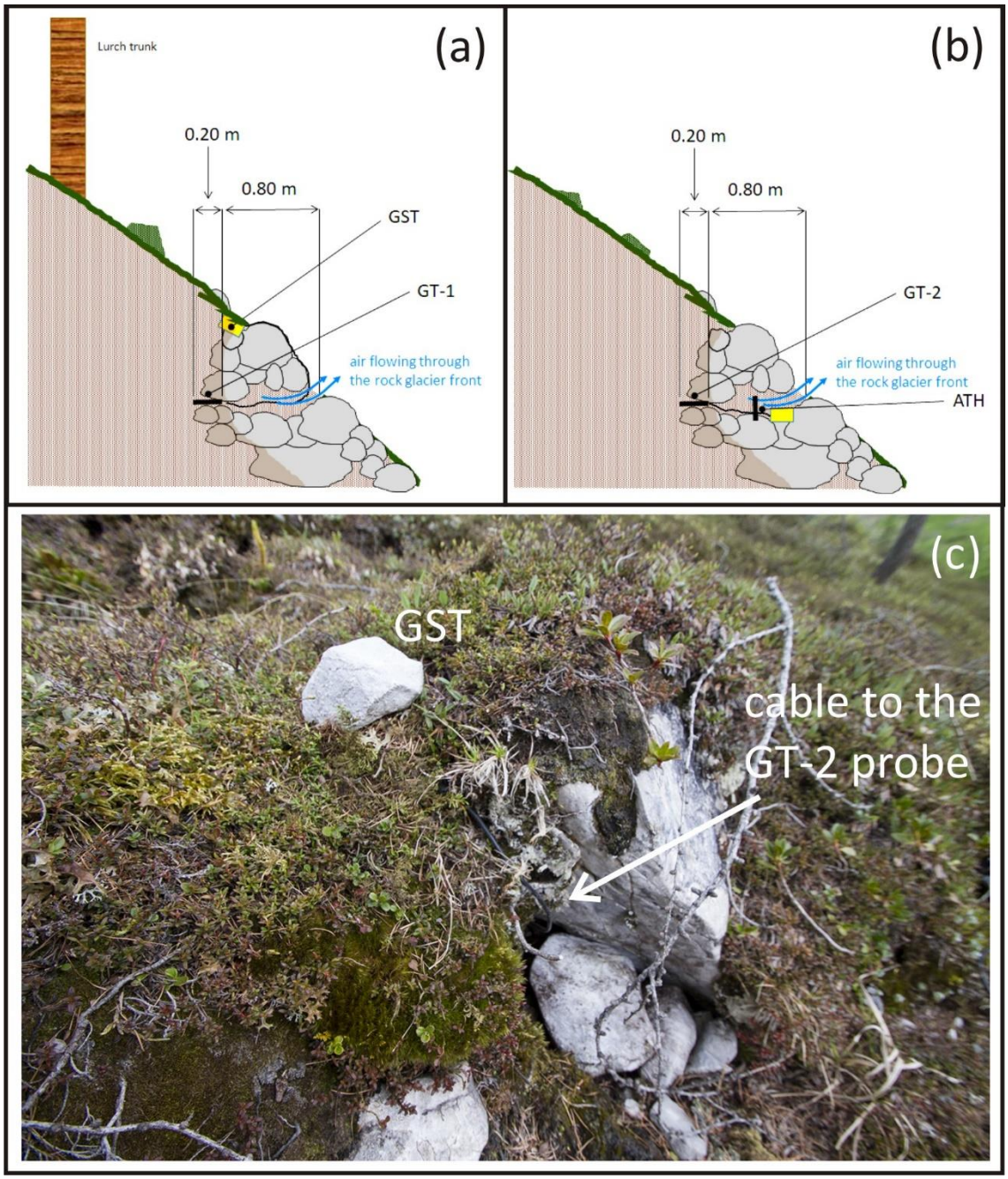

224

225 Fig. 2

226 Location of the ground temperature probes at the rock glacier front: a) details of the location 2 as
227 highlighted in Fig. 4a; b) details of the location 1 as highlighted in Fig. 4; c) photograph of the location 2
228 highlighting the GST monitoring site, i.e. the built-in sensor (not visible here) and the GT-2 located in the
229 small cavity at the rock glacier's front (Photo by R.R. Colucci). The sketches in a and b are intended to clarify
230 how the probes are inserted in the ground and the drawing is not correctly scaled both in terms of lengths
231 and steepness of the slope.

3.5 Electrical Resistivity Tomography (ERT)

Two longitudinal ERT profiles were acquired on the rock glacier (Fig. 4); one in 2015 (October 30th) and the other in 2016 (September 7th). The 2015 ERT survey was performed with a Syscal Pro georesistivimeter (IRIS International) connected to 72 electrodes with a 2 m spacing. We used both standard Wenner (W) and Wenner-Schlumberger (WS) electrode configurations, obtaining 828 and 1221 measures, respectively. After the preliminary analysis on 2015 ERT data we decided to enlarge the electrode spacing to 5 m for the 2016 survey. In 2016, we used a Pasi 16GL-N instrument with a standard Wenner configuration to collect two partially overlapping profiles, each of them with 32 electrodes. During the processing we concatenated such profiles obtaining a 48 electrodes (235 m long) profile with 289 resistivity values. Each measure was repeated from three to six times, depending on the standard deviation of the collected values, then stacking the data, to minimize random noises. The overall high data quality is confirmed by the very low standard deviation between reciprocal measurements: 8 values from 2015 W profile, 7 values from 2015 WS profile and only 4 values from 2016 W profile have RMS error above 0.5%.

After careful data editing by checking the effective electric currents, self potentials, difference of potential, and apparent resistivities, we used Res2Dinv software (Loke and Dahlin, 2002) to invert the data and set a RMS convergence limit equal to 5%. Due to the high quality of the data neither interpolation nor resistivity constrains have been applied. On the other hand, it was almost impossible to follow a straight line on the field, especially for the 2016 profile. Therefore, we recalculated all the geometrical factors by using the actual electrodes locations measured by an RTK GPS device, which allowed a centimetric accuracy. The RMS mean error obtained after data inversion is always lower than 10% after maximum 5 iterations, despite the very rough topography and the logistical problems, related to the connection of some of the electrodes into the ground.

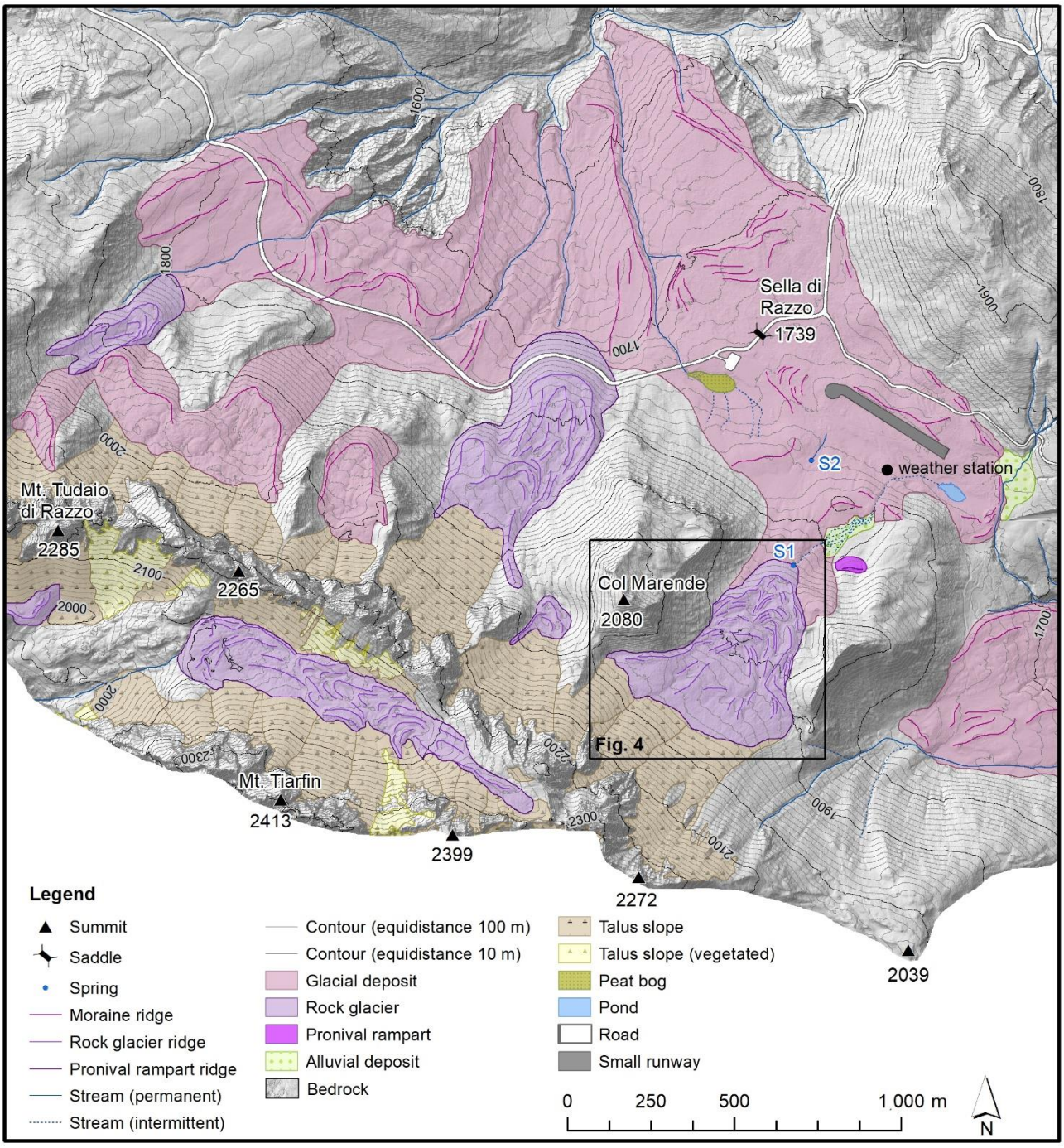

Fig. 3

Geomorphological map of the broader study area, characterized by high density of rock glaciers and moraines. The RRG is marked with a black square shown in detailin Fig. 4. The base map and contours are realized from a high resolution (2x2 m cell) DEM kindly made available by the Geological Service of the Veneto Region.

3. Results

4.1 Geomorphology of the study area

The landscape of the study area (Fig. 3) is largely characterized by typical alpine glacial and periglacial landforms. The carbonate slopes below the highest mountain crests are mainly covered by non-vegetated talus deposits, generally directly linked to the rock glaciers located downwards. Lateral, frontal and hummocky moraine ridges cover less steep slopes immediately below the rock glaciers and are stratigraphically older than the rock glaciers. Till cover is are occasionally dissected by permanent or intermittent streams flowing from the rock glaciers terminus over moraines and towards north. The area to the north forms a badland-like landscape, which is extensively eroded by water. Moraine ridges are a few meters high and likely designate several glacier stabilizations (stadials) during the Late glacial and/or early Holocene periods. As recently shown by Colucci et al. (2014), the LGM ELA in the southeastern Alps was much lower than the LGM ELA in the Casera Razzo area, which likely acted as an area of accumulation for larger glaciers. Ten rock glaciers (6 of them shown in Fig. 3) with a total area of 0.7 km^2 were mapped in the Tiarfin group (Fig. 3). They extend between 2,280 and 1,680 m asl. Seven of them are tongue-shaped, while the rest have a lobate geometry. Their areas vary between 5,410 and 189,429 m^2. The RRG is located SE of the Col Marende peak (Fig. 3) and its rooting zone is located on the NE slopes of the Tiarfin group. It has all the characteristics of a tongue-shaped rock glacier with a length/width ratio of 1.9. The altitudinal difference between the maximum (1,981 m asl) and minimum (1,831 m asl) point is 150 m, while the median elevation is 1,909 m. The area covered by this landform is ca. 173,000 m^2. The height of the frontal slope is ca. 30 m and the mean and maximum slope angles of the front are 30° and 43°, respectively. The RRG surface is characterized by ridges composed of angular metric Triassic dolostone and limestone boulders, originating from the local slopes. The orientation of the ridges is related to the N-NE downward direction of the rock glacier movement. Between the ridges, thermokarst depressions are formed mainly on the main body and towards the front, but not over it. The RRG is entirely and extensively covered by vegetation, with prevailing *Pinus mugo* and *Larix decidua*, while the vegetation at the front is much different from the surroundings and appears to be related to locally colder thermal regime with species

typical of higher altitudes as the *Cladonia macrophyllodes Nyl.* (Tretiach, 1992; Nimis et al., 2018;). At the contact between the rock glacier front and the bedrock a spring emerges, from which an intermittent stream, active mainly in spring and early summer, flows towards a depression behind a frontal moraine. There, a pond forms and usually persists until the early summer. Other springs, which are not located immediately below the RRG front, but clearly feed from the rock glacier area, are present NW of the front, in the area of moraine deposits.

According to Equation 1, the mean thickness of the RRG (debris and ice) in its active state would be 35.2 m. This results in a total rock glacier volume of $6.08*10^6$ m^3 and volumetric ice content between $2.43*10^6$ and $3.65*10^6$ m^3 if considering a range of 40–60% for the ice content. Thus, the water volume equivalent was calculated to be between $2.19*10^6$ m^3 and $3.28*10^6$ m^3.

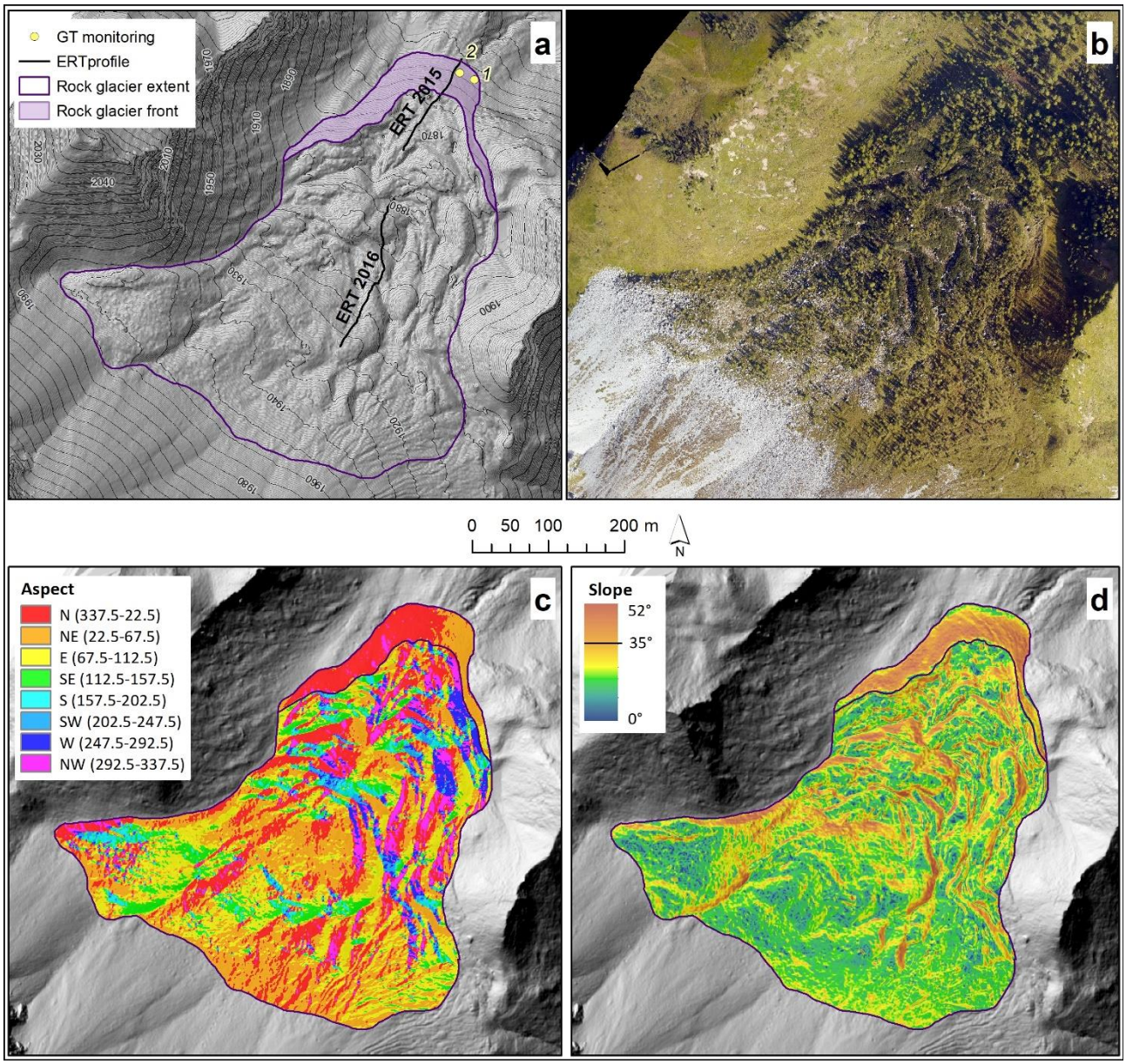

Fig. 4

(a) The extent of the RRG with the location of ERT profiles performed in 2015 and 2016, and ground temperature monitoring locations 1 and 2 (details in Fig. 2). (b) Orthophoto of the RRG area. Note the dense vegetation cover over the entire surface of the rock glacier. (c) Aspect map and (d) slope map of the area covered by the RRG. Base layer for (a), (c) and (d) is a shaded relief extracted from the 2016 1-m DTM.

4.2 Climatology of the area

The 1981–2010 climatology of MAAT at 2,200 m asl in the south eastern Alps, recently reconstructed by Colucci and Guglielmin (2015), is in very good agreement with the data record of 2004-2017 monthly mean temperature in Sella di Razzo (R=0.95; Fig. 5a), as well as with the data record of Mt. Zoncolan (Fig. 1b) meteorological station (R=0.95). Therefore, it was possible to reconstruct the 1981-2010 MAAT for Sella di Razzo when data was missing. A 37-year-long record of MAAT is presented in Fig. 5b. MAAT in Sella di Razzo, which is located very close to the front of the rock glacier (Fig. 3), is 3.7°C (σ=0.7). Indeed, this 30-year-long period has been characterized by a steep and accelerated warming during which MAAT increased by about 1.0°C. Temperature data from Sella di Razzo shows a steep rising trend with three of the warmest year recorded in the last five years of observation, which is in accordance with observations in the southeastern Alps. The year 2015 is the warmest of the Sella di Razzo record and likely the warmest of the last (at least) 150 years.

Mean annual precipitation (MAP) over the period 1961-2000 recorded at the meteorological station of Sauris at 1,212 m asl was 1543 mm water equivalent (w.e.). February is the driest month (74 mm w.e.) and October is the wettest (175 mm w.e.). More recent observations (2005-2017) performed in Forni di Sopra (Fig. 1b) at 922 m asl point to similar data with MAP of 1548 mm w.e. (January 84 mm w.e.; November 176 mm w.e.).

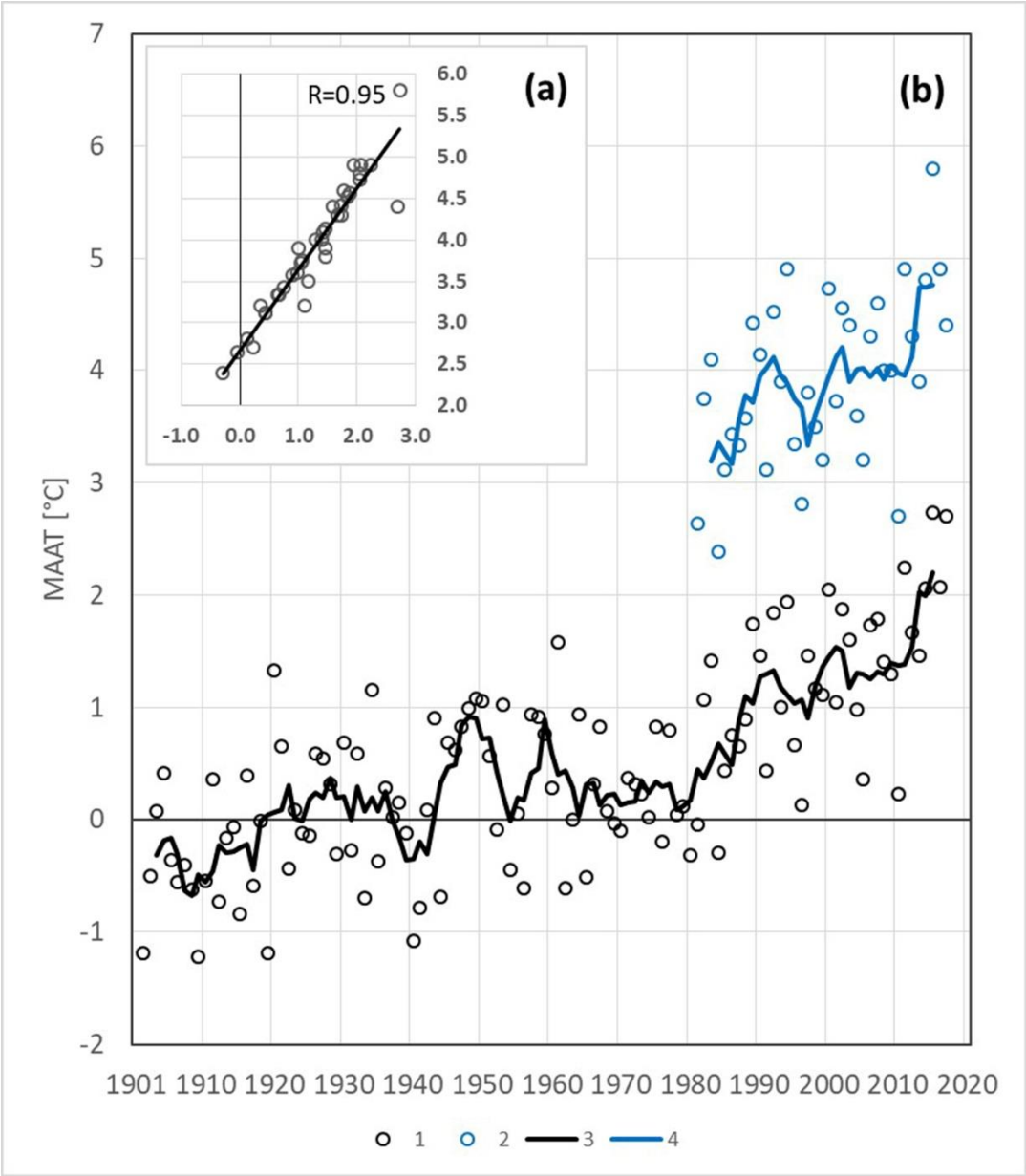

Fig. 5

In a) scatter plot of temperature reconstruction from Julian Alps (Colucci and Guglielmin, 2015) and Sella Razzo dataset. In b) 1901-2017 climatology of: (1) MAAT Canin (2,200 m asl); (2) MAAT Sella Razzo (1,839 m asl); (3) 5-year centered running mean for Canin; (4) 5-year centered running mean for Sella Razzo.

4.3 Geomorphic Changes and Analysis

By analysing the LiDAR point cloud data from 2009 and 2016, some small changes in the area of interest (AOI; corresponding to the rock glacier extent) were detected (Table 2). A net volume change of -1803 m3 and the average net thickness (computed as the total net volume difference divided by the AOI) of 1 cm for the period 2009-2016 was found. The percentage of the AOI with detectable changes (i.e. exceeding the minimum level of detection) equals 2%. All these values clearly show that geomorphic changes in the area of interest are negligible along all (x,y,z) directions.

	Thresholded DoD Estimate
Negative volume change (m^3)	2065
Positive volume change (m^3)	262
Net volume change (m^3)	-1803
Average depth of negative change (m)	0.84
Average depth of positive change (m)	0.71
Percentage of AOI with detectable change	2%
Average net thickness difference for AOI (m)	-0.01

Table 2.

Statistics related to changes in the area of interest (AOI), computed on the thresholded DoD.

4.4 Results from temperature monitoring

A 36-month-long record of continuous semi-hourly ground (GT-1 and GT-2), soil (GST) and air-flow (AT-H) temperatures were recorded from August 2015 to July 2017 at the front of the RRG (Fig.s 2 and 4). GST shows a marked daily variability in summer with diurnal excursions often greater than 25 °C. Daily maximums exceeded 30°C in several occasions during the summers of 2016 and 2017 with a peak of 35.4°C

in 2017. GT-1 and GT-2 show a similar pattern in all the seasons with a fast decreasing trend from early autumn to mid winter and a slow and long rising trend from mid winter to the end of the summer. AT-H is in phase with GT-2, but shows warmer temperature during the winter/early spring phase. At the onset of the snowmelt season in March, temperature at all the locations rapidly rise to 0°C and a long zero curtain effect is recorded. In autumn a less pronounced zero curtain phase is also observed in 2016 and 2017, especially at locations GT-2 and AT-H. The coldest temperature generally occurs on early-to-mid winter, when minimum peaks between -15°C and -20°C have been recorded and associated with low snow cover (Fig. 5). In winter 2018, early snow cover dumped the cooling of the ground, which only occasionally reached minimum values around -5°C ("S" in Fig. 5). Only the GST location shows a positive mean annual temperature (MAT; Fig. 6), whilst at location GT-1 MAT is the lowest (Fig. 6).

The temperature of the spring immediately below the rock glacier front (S1 in Fig. 3;) was measured to 1.3°C on the 19th of June 2016, when the air temperature was 9.0°C and winter snow cover was completely absent in the area and over the rock glacier. The spring S2 (Fig. 3;), ~300 m far from the rock glacier front and 40 m lower in elevation from the S1 had a temperature of 2.7°C on the same day.

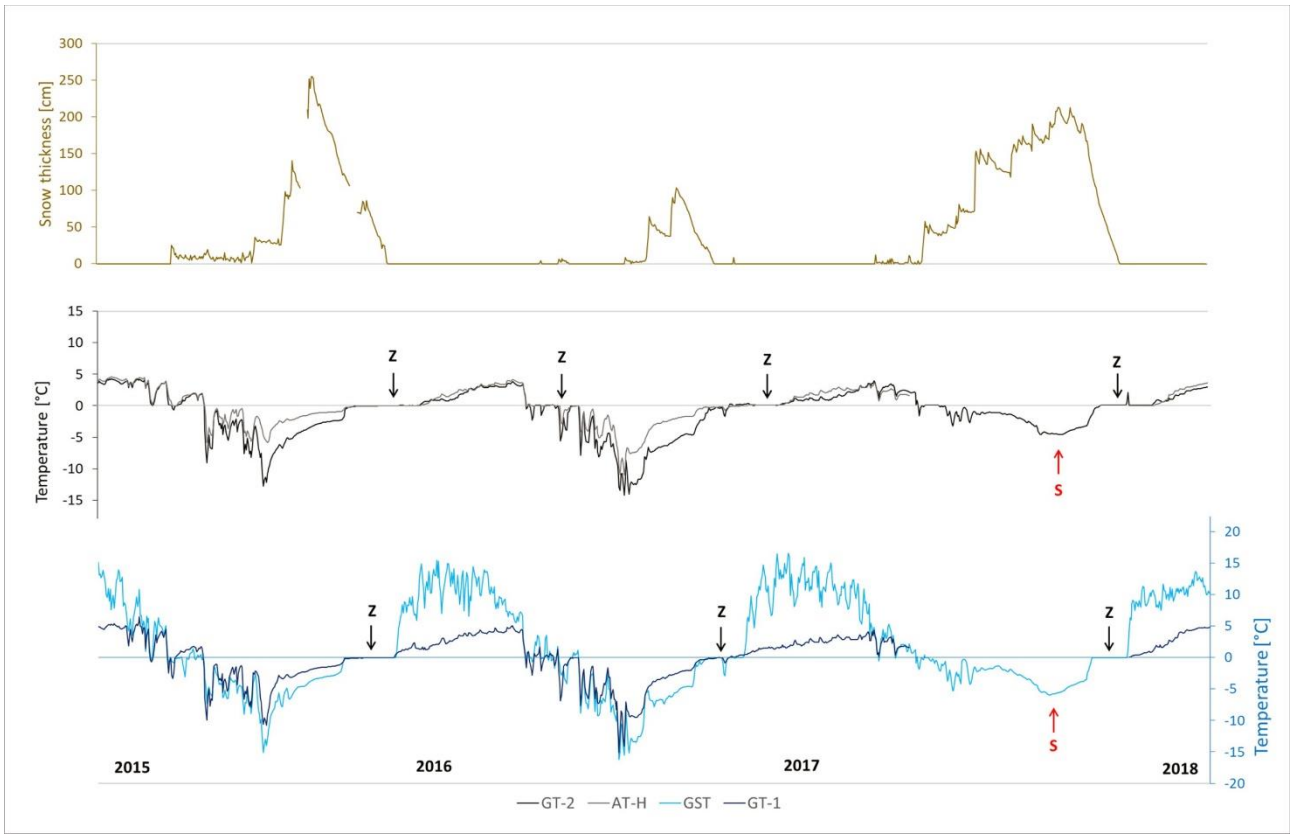

Fig. 6

Daily ground temperature data at the rock glacier front and snow thickness at the Sella Razzo meteorological station (see Fig. 3 for location): with "z" the "zero curtain" phases are highlighted; with "s" the thick snow cover of the winter season 2017-18, which has inhibited the ingression of cold air into the ground, is also highlighted. First data refers to 8th August, 2015 while last data belongs to 15th August, 2018. See Fig. 2 for the location of the probes. GT represents the ground surface temperature, AT-H the temperature of the air flowing in the small cavities and GST is the ground surface temperature.

	GST	GT-1	GT-2	ATH
jan	-7.53	-6.75	-5.67	-7.70
feb	-5.25	-4.88	-2.61	-3.29
mar	-4.14	-3.81	-1.30	-1.67
apr	-1.00	-1.15	-0.29	-0.24
may	2.36	0.10	0.01	0.40
jun	10.00	0.26	0.17	1.37
jul	11.48	1.03	1.66	2.50
aug	11.39	2.73	3.21	3.90
sep	6.29	3.21	3.33	3.65
oct	1.56	1.19	1.07	0.71
nov	-1.32	-0.89	-0.34	-1.37
dec	-4.39	-3.25	-2.25	-3.74
		2 years		
		3 years		
MAT	1.62	-1.02	-0.25	-0.46

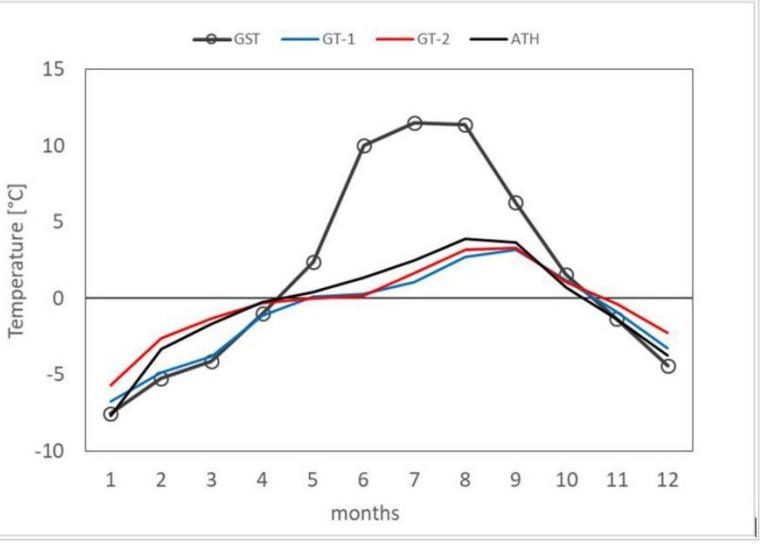

374

375 Fig. 7

376 Monthly and annual (MAT) ground and air temperature data at the RRG front. Grey boxes highlight
377 locations with “just” 2 continuous years of data recorded.

378

379 *4.5 ERT results*

380 Inverted 2015 ERT profiles show a resistivity range between about 0.3 and 40 kOhm·m (Fig. 7) with only
381 minor differences between WS (Fig. 8a) and W (Fig. 8b) configurations. In fact, for increasing depths a low
382 resistivity layer with variable thickness from about 2 up to 10 m is followed by a quite laterally continuous
383 zone with resistivity always above 10 kOhm·m and a maximum thickness of about 15 m. In the central part
384 of the 2015 profile (Fig. 8) there is a remarkable resistivity decreasing down to values of few hundreds
385 Ohm·m. Such results are similar to the ones obtained in the 2016 survey (Fig. 9), where, despite higher
386 overall resistivities, the above described trend is similar.

387 The higher resolution provided by the WS profile with respect to the W one (Figs. 8a and 8b, respectively)
388 shows very shallow and small high-resistivity-zones, shown by the black arrows in Fig. 8a. These zones
389 which might be related to local air filled fissures and small cavities just below the largest boulders are
390 especially obvious in the lower ridge (R1).

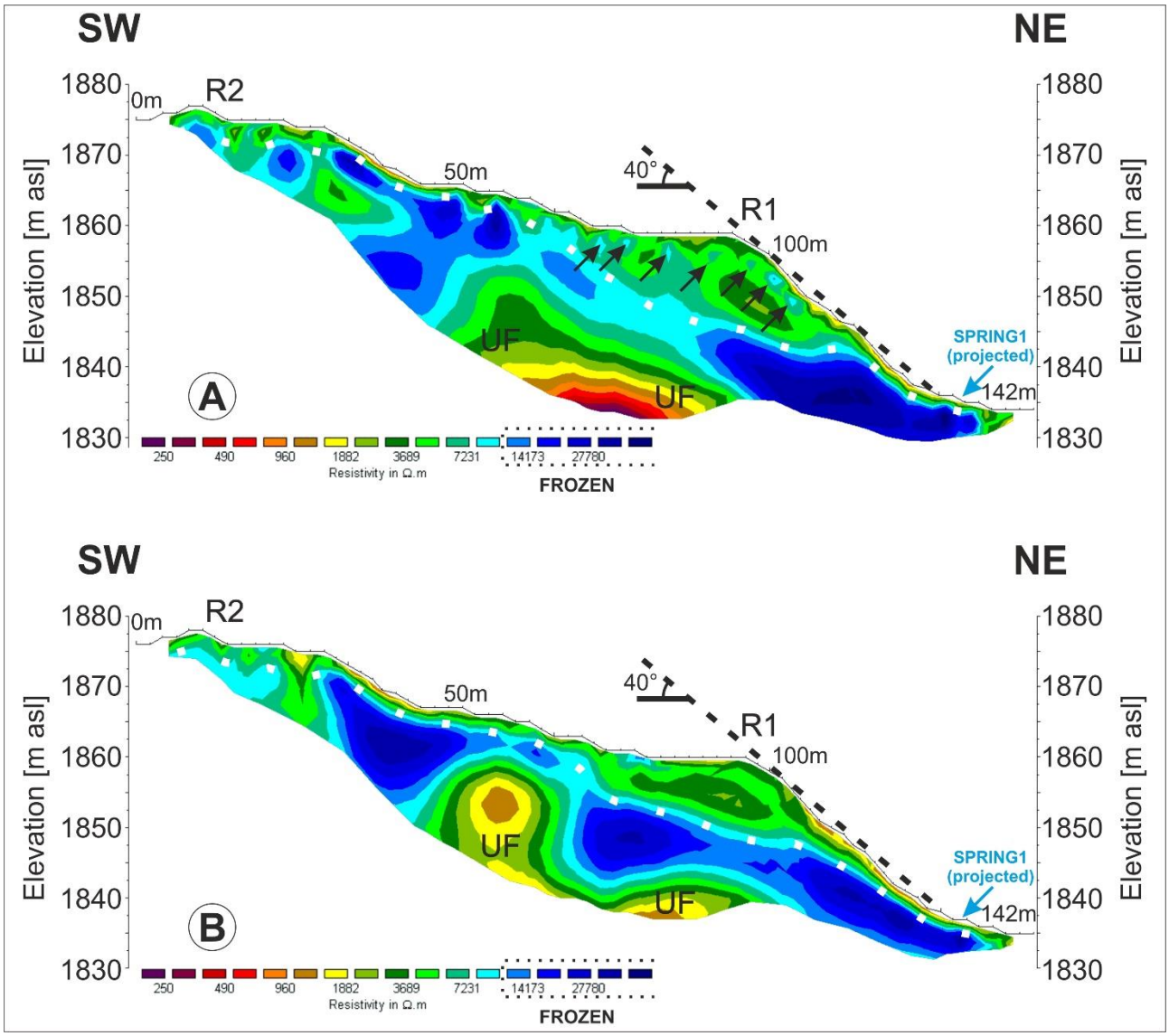

391

392 Fig. 8

393 Inverted ERT Wenner-Schlumberger (A) and Wenner (B) 2015 profiles. Black arrows mark surficial relatively
394 high resistivity zones, interpreted as air filled voids between rock blocks, the white-dotted line highlights
395 the approximate base of the active layer, and R1 and R2 highlight the two main ridges intersected by the
396 profile. Percentual RMS errors are equal to 9.9 and 6.9 for A) and B), respectively. Vertical to horizontal
397 ratio is equal to 1.

398

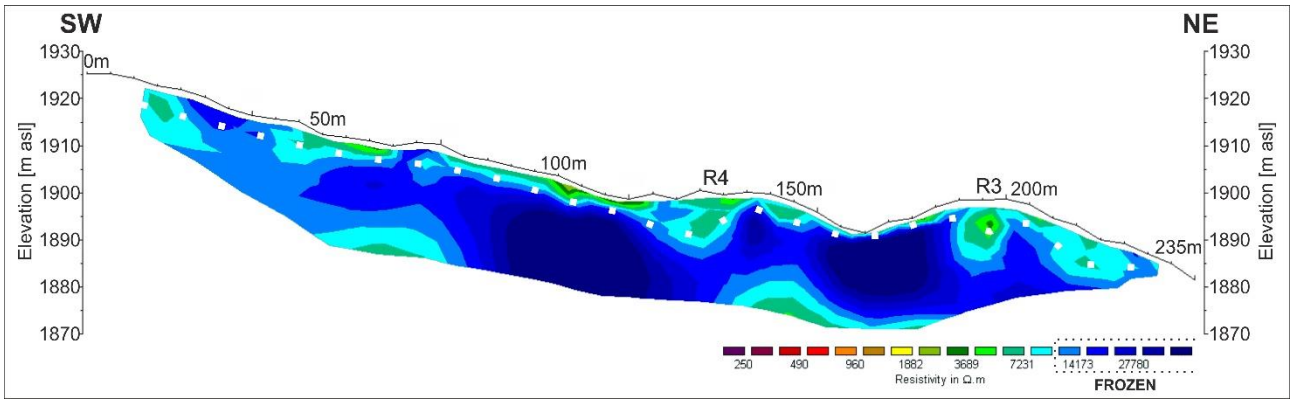

399

400 Fig. 9

401 Inverted ERT Wenner 2016 profile plotted with the same resistivity scale as in Fig.-5. White dotted line
402 highlights the approximated base of the active layer, while R3 and R4 labels highlight the two main ridges
403 intersected by the profile. Percentual RMS error is equal to 4.6. Vertical to horizontal ratio is equal to 1. The
404 exact location of this profile within the rock glacier indicated in Fig. 4a as ERT 2016.

405

406 **5. Discussion**

407 The RRG, which on the basis of our results is classified as inactive, would have been certainly classified as a
408 relict rock glacier according to the criteria presented in Table 4 and by using only remote sensing
409 techniques (aerial photographs, analysis of a more geometrically consistent DEM obtained from TLS, LiDAR
410 or photogrammetric surveys). Much of the RRG geomorphic characteristics, such as a concave median
411 longitudinal profile, a generally depressed body, no ice exposures, the presence of some collapsed features
412 (conical depressions) and a gentle transition to upper surface, would exclude the presence of ground buried
413 ice or interstitial ice. Additionally, when considering the MAAT of the last 37 years (3.7°C), we can infer that
414 the rock glacier is climatically located out of the range of a periglacial environment. The steepness of the
415 front of the RRG indeed might point to an active landform, but recent studies show possible higher external
416 angle of repose for limestone scree, generally in the range 35 - 45 ° with variability affected by factors, such
417 as the size distribution of clasts, cleanliness and moisture content (Oates, 1998; Rackl and Grötsch, 2018).

418 Several authors would consider this rock glacier as a relict one also on the basis of the present vegetation
419 cover.

420

Classification	RSD	RSD	RSD	RSD	RSD	RSD	CD	CD
Active	Steep front (>35°) and side slopes [1,2]	Surface with well defined furrows and ridges[1,3]	Median longitudinal profile is convex[4]	Swollen body[5]	eventual ice exposures[6]	Sharp crested frontal slope[7]	MAAT < -2°C[8]	Frozen material or ice core detectable at depths lower than ZAA[4]
Relict	Gently sloping (<30°)[1,2]	**(Naturally subdued) surface relief of ridges and furrows is still visible[1,3]**	**Median longitudinal profile is concave[4]**	**Depressed or flattened body[5]**	**No ice exposures and surface collapsed features[6]**	**Gentle transition (rounded crest) to upper surface[7]**	**MAAT >3°C[8]**	Frozen material or ice core detectable at depths higher than ZAA[4]

421 Table 4.

422 Remote Sensing Derived (RSD) and Climatically Derived (CD) classification for active and relict rock glaciers.
423 1) Barsch (1988); 2) Jones et al. (2018); 3) Kääb and Weber (2004); 4) Colucci et al. (2016); 5) Seppi et al.
424 (2004); 6) Janke (2013); 7) Wahrhaftig and Cox (1959); 8) French (2018). The characteristics of the RRG are
425 shown in bold.

426 On the other hand, the findings from this case study point to a widespread and abundant presence of
427 buried ice in the RRG, therefore indicating it should be classified as an inactive rock glacier. Specifically, ERT
428 inversions show resistivity values typically encountered in active rock glaciers. It is worth noting that for
429 both ERT profiles the resistivity exhibits thicker low sub-surficial zones below the ridges (labels R1-R4 on

Fig.s 8 and 9), while some high resistivities are also close to the topographic surface (up to about 2-2.5 m) in correspondence with the furrows. A similar distribution pattern, which should be related to colder temperatures in the furrows due to topographic or microclimatic effects, is reported by Harris and Pedersen (1998) and Hoelzle et al. (1999). An opposite behavior, likely caused by local compression phenomena in the ridge zones, is described by Hauck and Kneisel (2008) and Emmert and Kneisel (2017). The active layer thickness (ALT) varies between about 2 and 8 m (white dotted lines in Fig.s 8 and 9) showing a correspondence with the main ridges (R1, R2, R3, R4). The longitudinal lateral variability, shown by the electrical resistivity data along an almost continuous, more than 500 m long longitudinal profile (see Fig. 4) on the rock glacier, is overall small, demonstrating a generally increasing trend towards higher elevations. A relevant exception is represented by the well-defined shallow high resistivity zone at the rock glacier's front (Fig. 8), ending at its limit. The resistivity values exceeding 30 KOhm·m and the mean slope of the rock glacier's front along this profile is >35° (Fig. 4d), indicate the probable presence of ice-rich materials and permafrost conditions even at that location.

Additional ERT data, acquired from the plain just to the north of the rock glacier and not reported in this paper ,show a maximum resistivity of 2.5 KOhm·m, indirectly demonstrating that the ice-rich materials lie only within the rock glacier.

The cryological interpretation of the resistivity values in the absence of boreholes or other geophysical investigations is not easy to interpret, but according to Haeberli and VonDer Mühll (1996) values above 10-15 KOhm·m can be referred to rock glacier permafrost, whereas sedimentary ice has values close to or higher than 100 KOhm·m, showing high variability for low temperature conditions.

In more recent papers, Ribolini et al. (2010) studied the Foscagno rock glacier (Central Alps) and interpreted zones with resistivity exceeding 20 kOhm·m as *ice-rich permafrost* , while Emmert and Kneisel (2017) analyzed two rock glaciers in the Swiss Alps and fixed a resistivity threshold of 8 kOhm·m as the lower limit for the frozen state. Similar results are provided by Ikeda and Matsuoka (2006) by validating ERT data with direct observations in a trench and considering the differences between boulder and pebble sized rock glaciers. However, we have to consider that the presence of liquid water can strongly influence the

456 resistivity values (Hauck and Kneisel, 2008) and the grain size vertical and lateral variability also plays a role
457 (Kneisel et al., 2008), making it difficult to extrapolate a single resistivity threshold to infer the ice presence.
458 Summarizing and integrating the geophysical and geomorphological results from RRG, large portions of the
459 rock glacier contain ice, without relevant layers composed of massive ice, but rather with ice in pore spaces
460 and local, but continuous ice lenses. Although massive ice cannot be inferred by the resistivity values never
461 exceeding some tens of KOhm·m, the ice is widespread and continuous enough to generate an essentially
462 uninterrupted high resistivity level. The active layer consists of boulders (up to several meters wide) as well
463 as fine-grained sandy-silty materials as typically found in the Alps (Isaksen et al., 2000). Geophysical
464 investigations in the RRG also show the occurrence of frozen material during the summer and autumn
465 above the depth of zero annual amplitude (ZAA). In this type of deposit it is reasonable to hypothesize that
466 the ZAA, which represents the soil-and-climate-dependent depth where the annual variation is less than
467 0.1°C, at depth ≥ 15 m (Harris et al., 2009). Therefore, we infer the presence of frozen material in the RRG
468 related to current ground cryotic conditions.

469 Observations of both ground and spring water temperatures, and of air flows also support the hypothesis
470 that ice exists within this rock glacier. Recorded Mean Annual Ground Temperature (MAGT) points to the
471 presence of permafrost (Cremonese et al., 2011). Short periods of strong ground overcooling are
472 detectable from October-November up to the second half of January, generally with low snow cover on the
473 ground (Fig. 6). This is probably due to the warmer and less dense air than the external, flowing away from
474 the upper part of the rock glacier due to its buoyancy through voids between blocks and the debris (i.e.
475 chimney effect; (Thury, 1861; Balch, 1900)). This produces a negative low (lower air pressure) inside the
476 rock glacier, which triggers a forced aspiration of atmospheric air in the lower part of the rock glacier as
477 already highlighted by several authors (e.g., Morard et al., 2008; Popescu et al., 2017). This is clearly
478 detectable at the RRG from the AT-H probe, which shows the lowest mean monthly values in December
479 and January (Table 3). On the other hand, during summer months, colder and denser air flows out from the
480 rock glacier front, keeping cooler conditions at the rock glacier terminus and just in front of it. Mean and
481 absolute temperature observed at the RRG's front (Figs. 6 and 7) are largely consistent with previous

482 studies in the Alps on talus slopes (e.g., Delaloye and Lambiel, 2005; Popescu et al., 2017) and rock glaciers
483 (e.g., Delaloye and Lambiel, 2005; Morard et al., 2008), as well as in talus-and-gorge ice caves in North
484 America (Holmgren et al., 2017).

485 With such evidence, cryotic conditions in the ground are still currently occurring here. This means that the
486 forced lowering of the mean annual ground temperature in turns allows permafrost conditions to reach
487 much lower elevations compared to the regional climate limits. Similar cases exist in the Mediterranean
488 areas and in North Africa, where the presence of permafrost is marginal. This is for instance the case of
489 Morocco, where ground temperature measurements imply that permafrost may still be present (Vieira et
490 al., 2017).

491

492 By overlying the Alpine-wide Permafrost Model (APMOD, Boeckli et al., 2012) on the geomorphological
493 map of the area of Casera Razzo (Fig. 10), we observed that the area of possible presence of permafrost is
494 900 m lower than that modeled in the area around the RRG. Considering the cooling effect cause by coarse-
495 blocky rock glaciers in the Alps, the offset found in the RRG area is actually greater than that reported in
496 Boeckli et al. (2012) In their “debris model”, a maximum altitudinal variation offset from APMOD between -
497 153 m to +770 m is assumed. However, the same authors warn about possible larger differences related to
498 local permafrost patches in densely vegetated areas or below the tree line (as the present case), which are
499 not considered in the model.

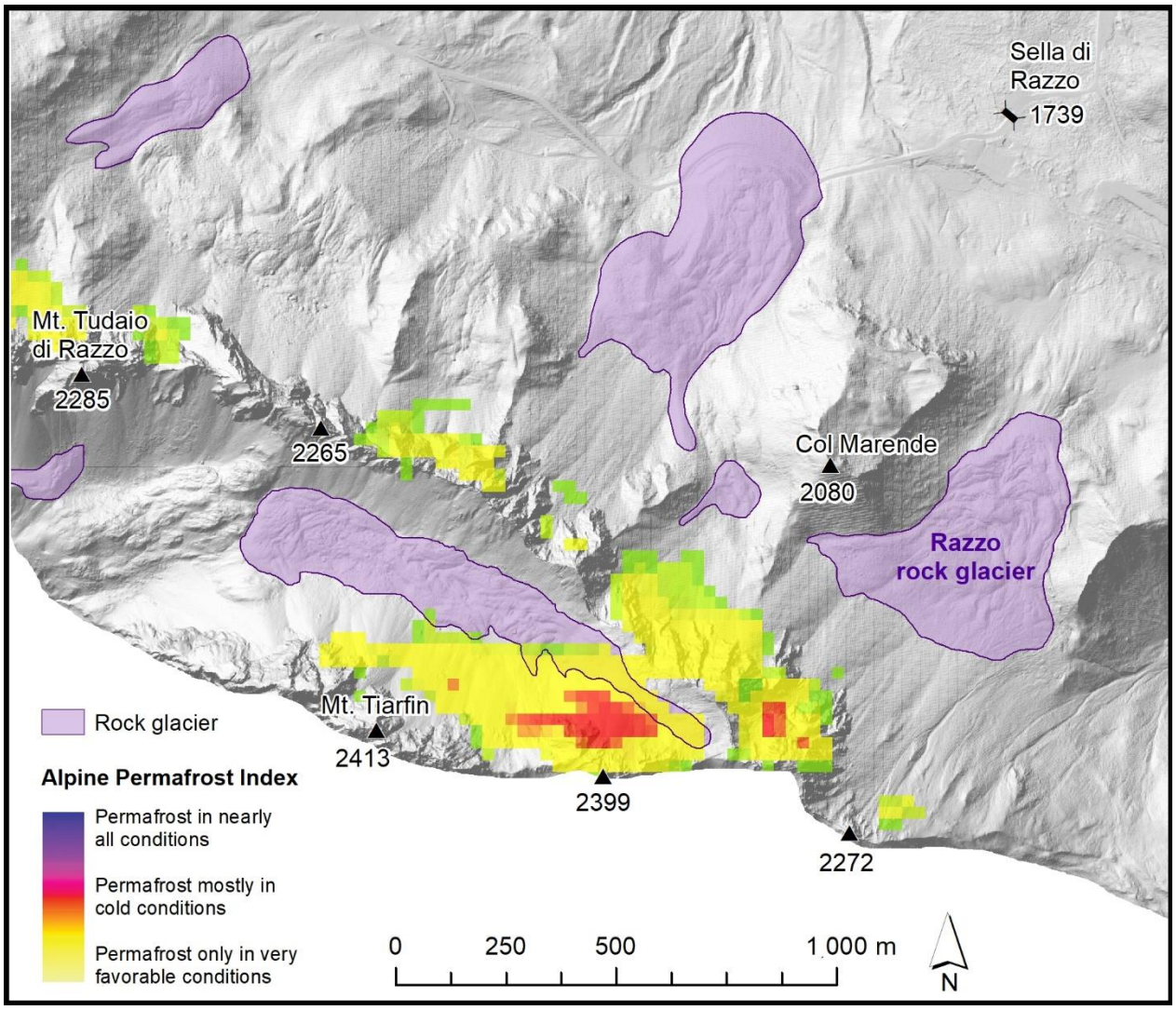

Fig. 10. Permafrost distribution in the Casera Razzo area according to the Alpine permafrost index map (Boeckli et al., 2012). Permafrost conditions are envisaged on the north facing slopes above the RRG, and in the talus scree and part of a rock glacier located at higher elevation.

6. Conclusions

This work shows that rock glaciers considered relict on the basis of remote sensing and geomorphological evidence can still contain residual ice at elevations much lower than the modelled permafrost limit. Indeed rock glaciers can exist at altitudes several hundred meters lower than forecasted by modeling techniques or taking into account the -2°C isotherm. This aspect is of particular interest because it shows how models can be inaccurate when dealing with sporadic permafrost areas. Several examples exist from the

Mediterranean mountains, where under thick debris cover (rock glaciers) and in caves (permanent ice deposits in caves) no model or index is currently able to predict the presence of ice. This is particularly true for high altitude karstic terrains, where the occurrence of ground ice in caves is common. Several ice caves exist in the area of the RRG (Colucci et al., 2016b, 2017), in the southern Alps, in the Apennines and Sicily in Italy (Maggi et al., 2018) and in other Mediterranean areas such as Greece (e.g., Pennos et al., 2018).

As a result, caution should be applied when calculating physical parameters such as the minimum altitudinal limit for the occurrence of permafrost at regional scales, the volume of water equivalent in a geographic area affected by possible permafrost conditions, as well as paleoclimatic reconstruction of permafrost occurrence and predictions of future scenarios.

Acknowledgments

This research is partially funded by the "Progetti di Ricerca di Rilevante Interesse Nazionale – PRIN 2015", grant number: 2015N8F555. The C3 project (www.c3project.net) supported LiDAR data acquisition performed in 2016. Daniele Fontana and Veronica Franco are aslo deeply acknowledged for their support during fieldworks. Matteo Spagnolo and an anonymous reviewer, are deeply acknowledged for their very useful suggestions made on an earlier version of this paper. We also thank the Editor Achim A. Beylich for further comments and suggestions and Neil Glasser for the English revision.

References

Anderson, R.S., Anderson, L.S., Armstrong, W.H., Rossi, M.W., Crump, S.E., 2018. Glaciation of alpine valleys: The glacier – debris-covered glacier – rock glacier continuum. Geomorphology 311, 127–142. https://doi.org/10.1016/j.geomorph.2018.03.015

Arcone, S.A., Lawson, D.E., Delaney, A.J., Strasser, J.C., Strasser, J.D., 1998. Ground-penetrating radar reflection profiling of groundwater and bedrock in an area of discontinuous permafrost. Geophysics 63, 1573–1584. https://doi.org/10.1190/1.1444454

Arenson, L.U., 2002. Unstable alpine permafrost: a potentially important natural hazard – variations of geotechnical behaviour with time and temperature, Doctoral Thesis. Institute for Geotechnical Engineering, Swiss Federal Institute of Technology ETH Zurich.

Balch, E.S., 1900. Glacières or Freezing Caverns. Philadelphia Allen, Lane & Scott reprinted 1970 by Johnson Reprint Corp., New York.

Ballantyne, C.K., 2018. Periglacial Geomorphology. John Wiley and Sons Ltd., pp. 472.

Baroni, C., Bondesan, A., Chiarle, M., 2017. Relazioni della campagna glaciologica 2016 (Report of the glaciological survey 2016). Geogr. Fis. e Din. Quat. 40, 233–319.

Barsch, D., 1996. Rockglaciers : indicators for the Present and Former Geoecology in High Mountain Environments. Springer-Verlag Berlin Heidelberg., pp. 331. https://doi.org/10.1007/978-3-642-800993-1

Barsch, D., 1988. Rockglaciers, in: Clark, M.J. (Ed.), Advances in Periglacial Geomorphology. John Wiley & Sons, Ltd, Chichester, pp. 69–90.

Barsch, D., Fierz, H., Haeberli, W., 1979. Shallow Core Drilling and Bore-Hole Measurements in the Permafrost of an Active Rock Glacier near the Grubengletscher, Wallis, Swiss Alps. Arct. Alp. Res. 11, 215–228. https://doi.org/10.2307/1550646

Berthling, I., 2011. Beyond confusion: Rock glaciers as cryo-conditioned landforms. Geomorphology 131, 98–106. https://doi.org/https://doi.org/10.1016/j.geomorph.2011.05.002

Boeckli, L., Brenning, A., Gruber, S., Noetzli, J., 2012. Permafrost distribution in the European Alps: Calculation and evaluation of an index map and summary statistics. Cryosphere 6, 807–820. https://doi.org/10.5194/tc-6-807-2012

Brenning, A., 2005. Climatic and geomorphological controls of rock glaciers in the Andes of Central Chile. Humboldt-Universität zu Berlin, Mathematisch-Naturwissenschaftliche Fakultät II. https://doi.org/http://dx.doi.org/10.18452/15332

Cannone, N., Gerdol, R., 2003. Vegetation as an Ecological Indicator of Surface Instability in Rock Glaciers. Arctic, Antarct. Alp. Res. 35, 384–390. https://doi.org/10.1657/1523-0430(2003)035[0384:VAAEIO]2.0.CO;2

Capps, S.R., 1910. Rock Glaciers in Alaska. J. Geol. 18, 359–375.

Carulli, G.B., 2006. Carta geologica del Friuli Venezia Giulia. Scala 1:150,000.

Clark, D.H., Steig, E.J., Potter Noel, J., Gillespie, A.R., 1998. Genetic variability of rock glaciers. Geogr. Ann. Ser. A, Phys. Geogr. 80, 175–182. https://doi.org/10.1111/j.0435-3676.1998.00035.x

Colucci, R.R., Monegato, G., Žebre, M., 2014. Glacial and proglacial deposits of the resia valley (ne Italy): New insights on the onset and decay of the last alpine glacial maximum in the Julian Alps. Alp. Mediterr. Quat. 27, 85–104.

Colucci, R.R., Guglielmin, M., 2015. Precipitation–temperature changes and evolution of a small glacier in the southeastern European Alps during the last 90 years. Int. J. Climatol. 35, 2783–2797. https://doi.org/10.1002/joc.4172

Colucci, R.R., Žebre, M., 2016. Late Holocene evolution of glaciers in the southeastern Alps. J. Maps 12, 289–299. https://doi.org/10.1080/17445647.2016.1203216

579 Colucci, R.R., Boccali, C., Žebre, M., Guglielmin, M., 2016a. Rock glaciers, protalus ramparts and pronival
580 ramparts in the south-eastern Alps. Geomorphology 269, 112–121.
581 https://doi.org/10.1016/j.geomorph.2016.06.039

582 Colucci, R.R., Fontana, D., Forte, E., Potleca, M., Guglielmin, M., 2016b. Response of ice caves to weather
583 extremes in the southeastern Alps, Europe. Geomorphology 261, 1–11.
584 https://doi.org/10.1016/j.geomorph.2016.02.017

585

586 Colucci, R.R., Luetscher, M., Forte, E., Guglielmin, M., Lanza, D., Princivalle, F., Vita, F., 2017. First alpine
587 evidence of in situ coarse cryogenic cave carbonates (CCCcoarse). Geogr. Fis. Din. Quat. 40, 53–59.
588 https://doi.org/10.4461/ GFDQ 2017.40.5 53-59

589

590

591 Cremonese, E., Gruber, S., Phillips, M., Pogliotti, P., Boeckli, L., Noetzli, J., Suter, C., Bodin, X., Crepaz, A.,
592 Kellerer-Pirklbauer, A., Lang, K., Letey, S., Mair, V., di Cella, U., Ravanel, L., Scapozza, C., Seppi, R.,
593 Zischg, A., 2011. Brief Communication: "An inventory of permafrost evidence for the European Alps."
594 Cryosph. 5, 651–657. https://doi.org/10.5194/tc-5-651-2011

595 Delaloye, R., Lambiel, C., 2005. Evidence of winter ascending air circulation throughout talus slopes and
596 rock glaciers situated in the lower belt of alpine discontinuous permafrost (Swiss Alps). Nor. Geogr.
597 Tidsskr. - Nor. J. Geogr. 59, 194–203. https://doi.org/10.1080/00291950510020673

598 Emmert, A., Kneisel, C., 2017. Internal structure of two alpine rock glaciers investigated by quasi-3-D
599 electrical resistivity imaging. Cryosph. 11, 841–855. https://doi.org/10.5194/tc-11-841-2017

600 French, H.M., 2018. The Periglacial Environment, 4th Editio. ed. John Wiley and Sons, Chichester, UK.

601 Giardino, J.R., Shroder, J.F., Vitek, J.D., 1987. Rock Glaciers. Allen & Unwin, London.

602 Guglielmin, M., Biasini, A., Smiraglia, C., 1997. The contribution of geoelectrical investigations in the
603 analysis of periglacial and glacial landforms in ice free areas of the northern foothills (northern victoria
604 land, antarctica). Geogr. Ann. Ser. A, Phys. Geogr. 79, 17–24. https://doi.org/10.1111/j.0435-
605 3676.1997.00003.x

606 Guglielmin, M., Camusso, M., Polesello, S., Valsecchi, S., 2004. An Old Relict Glacier Body Preserved in
607 Permafrost Environment: The Foscagno Rock Glacier Ice Core (Upper Valtellina, Italian Central Alps).
608 Arctic, Antarct. Alp. Res. 36, 108–116. https://doi.org/10.1657/1523-
609 0430(2004)036[0108:AORGBP]2.0.CO;2

610 Guglielmin, M., Lozej, A., Tellini, C., 1994. Permafrost distribution and rock glaciers in the livigno area
611 (Northern Italy). Permafr. Periglac. Process. 5, 25–36. https://doi.org/10.1002/ppp.3430050104

612 Guglielmin, M., Ponti, S., Forte, E., 2018. The origins of Antarctic rock glaciers: periglacial or glacial
613 features? Earth Surf. Process. Landforms 43, 1390–1402. https://doi.org/10.1002/esp.4320

614 Haeberli, W., 1985. Creep of mountain permafrost: internal structure and flow of Alpine rock glaciers.
615 Mitteilungen der Versuchsanstalt fur Wasserbau, Hydrol. und Glaziologie an der ETH Zurich 77, 5–142.

616 Haeberli, W., Hallet, B., Arenson, L., Elconin, R., Humlum, O., Kääb, A., Kaufmann, V., Ladanyi, B., Matsuoka,
617 N., Springman, S., 2006. Permafrost creep and rock glacier dynamics. Permafr. Periglac. Process.
618 https://doi.org/10.1002/ppp.561

619 Haeberli, W., Hoelzle, M., Kääb, A., Keller, F., Vonder Müll, D., Wagner, S., 1998. Ten years after drilling
620 through the permafrost of the active rock glacier Murtèl, Eastern Swiss Alps: Answered questions and
621 new perspectives. Permafr. - Seventh Int. Conf. 403–410.

Haeberli, W., Hoelzle, M., Paul, F., Zemp, M., 2007. Integrated monitoring of mountain glaciers as key indicators of global climate change: the European Alps. Ann. Glaciol. 46, 150–160. https://doi.org/10.3189/172756407782871512

Haeberli, W., VonDer Mühll, D., 1996. On the characteristics and possible origins of ice in rock glacier permafrost. Z. Geomorph. N.F. SuppI. 104, 43–57.

Harris, S., Pedersen, D., 1998. Thermal regimes beneath coarse blocky materials. Permafr. Periglac. Process. 9, 107–120. https://doi.org/10.1002/(SICI)1099-1530(199804/06)9:2<107::AID-PPP277>3.0.CO;2-G

Harris, C., Arenson, L.U., Christiansen, H.H., Etzelmüller, B., Frauenfelder, R., Gruber, S., Haeberli, W., Hauck, C., Hölzle, M., Humlum, O., Isaksen, K., Kääb, A., Kern-Lütschg, M.A., Lehning, M., Matsuoka, N., Murton, J.B., Nötzli, J., Phillips, M., Ross, N., Seppälä, M., Springman, S.M., Mühll, D.V., 2009. Permafrost and climate in Europe: Monitoring and modelling thermal, geomorphological and geotechnical responses. Earth-Science Rev. 92, 117–171. https://doi.org/https://doi.org/10.1016/j.earscirev.2008.12.002

Hauck, C., Böttcher, M., Maurer, H., 2011. A new model for estimating subsurface ice content based on combined electrical and seismic data sets. Cryosph. 5, 453–468. https://doi.org/10.5194/tc-5-453-2011

Hauck, C., Mühll, D.V., 2003. Inversion and interpretation of two-dimensional geoelectrical measurements for detecting permafrost in mountainous regions. Permafr. Periglac. Process. 14, 305–318. https://doi.org/10.1002/ppp.46

2

Hauck, C., Vonder Mühll, D., Maurer, H., 2003. Using DC resistivity tomography to detect and characterize mountain permafrost. Geophys. Prospect. 51, 273–284. https://doi.org/10.1046/j.1365-2478.2003.00375.x

Hauck, C., Kneisel, C., 2008. Quantifying the ice content in low-altitude scree slopes using geophysical methods, in: Hauck, C., Kneisel, C. (Eds.), Applied Geophysics in Periglacial Environments. Cambridge University Press, Cambridge, pp. 153–164.

Hausmann, H., Krainer, K., Brückl, E., Mostler, W., 2007. Internal structure and ice content of Reichenkar rock glacier (Stubai Alps, Austria) assessed by geophysical investigations. Permafr. Periglac. Process. 18, 351–367. https://doi.org/10.1002/ppp.601

Hoelzle, M., Wegmann, M., Krummenacher, B., 1999. Miniature temperature dataloggers for mapping and monitoring of permafrost in high mountain areas: first experience from the Swiss Alps. Permafr. Periglac. Process. 10, 113–124. https://doi.org/10.1002/(SICI)1099-1530(199904/06)10:2<113::AID-PPP317>3.0.CO;2-A

Holmgren, D., Pflitsch, A., Rancourt, K., Ringeis, J., 2017. Talus-and-gorge ice caves in the northeastern United States past to present—A microclimatological study. J. Cave Karst Stud. 79, 179–188. https://doi.org/10.4311/2014IC0125

Hughes, P.D., 2018. Little Ice Age glaciers and climate in the Mediterranean mountains: a new analysis. Cuad. Investig. Geográfica 44, 15–45. https://doi.org/http://dx.doi.org/10.18172/cig.3362

Hughes, P.D., Gibbard, P.L., Woodward, J.C., 2003. Relict rock glaciers as indicators of Mediterranean palaeoclimate during the Last Glacial Maximum (Late Würmian) in northwest Greece. J. Quat. Sci. 18, 431–440. https://doi.org/10.1002/jqs.764

Humlum, O., 2000. The geomorphic significance of rock glaciers: estimates of rock glacier debris volumes and headwall recession rates in West Greenland. Geomorphology 35, 41–67.

https://doi.org/https://doi.org/10.1016/S0169-555X(00)00022-2

Humlum, O., 1998. The climatic significance of rock glaciers. Permafr. Periglac. Process. 9, 375–395. https://doi.org/10.1002/(SICI)1099-1530(199810/12)9:4<375::AID-PPP301>3.0.CO;2-0

Ikeda, A., Matsuoka, N., 2006. Pebbly versus bouldery rock glaciers: Morphology, structure and processes. Geomorphology 73, 279–296. https://doi.org/https://doi.org/10.1016/j.geomorph.2005.07.015

Isaksen, K., Ødegård, R.S., Eiken, T., Sollid, J.L., 2000. Composition, flow and development of two tongue-shaped rock glaciers in the permafrost of Svalbard. Permafr. Periglac. Process. 11, 241–257. https://doi.org/10.1002/1099-1530(200007/09)11:3<241::AID-PPP358>3.0.CO;2-A

Janke, J.R., 2013. Using airborne LiDAR and USGS DEM data for assessing rock glaciers and glaciers. Geomorphology 195, 118–130. https://doi.org/https://doi.org/10.1016/j.geomorph.2013.04.036

Jones, D.B., Harrison, S., Anderson, K., Betts, R.A., 2018. Mountain rock glaciers contain globally significant water stores. Sci. Rep. 8, 2834. https://doi.org/10.1038/s41598-018-21244-w

Kääb, A., Weber, M., 2004. Development of transverse ridges on rock glaciers: field measurements and laboratory experiments. Permafr. Periglac. Process. 15, 379–391. https://doi.org/10.1002/ppp.506

Kellerer-Pirklbauer, A., 2008. Aspects of glacial, paraglacial and periglacial processes and landforms of the Tauern Range, Austria. Unpublished doctoral thesis. University of Graz.

Kellerer-Pirklbauer, A., Lieb, G.K., Kleinferchner, H., 2012. A new rock glacier inventory of the eastern European Alps. Austrian J. Earth Sci. 105, 78–93.

King, L., Fisch, W., Haeberli, W., Wächter, H.P., 1987. Comparison on resistivity and radio-echo soundings on rock glacier permafrost. Zeitschrift für Gletscherkd. und Glazialgeol. 23, 77–97.

Kneisel, C., Hauck, C., 2008. Electrical methods, in: Hauck, C., Kneisel, C. (Eds.), Applied Geophysics in Periglacial Environments. Cambridge University Press, Cambridge, pp. 3–27.

Kneisel, C., Hauck, C., Fortier, R., Moorman, B., 2008. Advances in geophysical methods for permafrost investigations. Permafr. Periglac. Process. 19, 157–178. https://doi.org/10.1002/ppp.616

Krainer, K., Bressan, D., Dietre, B., Haas, J.N., Hajdas, I., Lang, K., Mair, V., Nickus, U., Reidl, D., Thies, H., Tonidandel, D., 2015. A 10,300-year-old permafrost core from the active rock glacier Lazaun, southern Ötztal Alps (South Tyrol, northern Italy). Quat. Res. (United States) 83, 324–335. https://doi.org/10.1016/j.yqres.2014.12.005

Leopold, M., Williams, M.W., Caine, N., Völkel, J., Dethier, D., 2011. Internal structure of the Green Lake 5 rock glacier, Colorado Front Range, USA. Permafr. Periglac. Process. 22, 107–119. https://doi.org/10.1002/ppp.706

Lieb, G.K., Kellerer-Pirklbauer, A., Kleinferchner, H., 2012. Second rock glacier inventory (RGI2) of Central and Eastern Austria, link to Shapefile. Suppl. to Kellerer-Pirklbauer, Andreas; Lieb, Gerhard Karl; Kleinferchner, Harald A new rock glacier Invent. East. Eur. Alps. Austrian J. Earth Sci. 105(2), 78-93, http//www.univie.ac.at/ajes/archive/volume_105_2/kellerer_at_al_ajes_105_2.pdf. https://doi.org/10.1594/PANGAEA.869805

Lilleøren, K.S., Etzelmüller, B., 2011. A REGIONAL INVENTORY OF ROCK GLACIERS AND ICE-CORED MORAINES IN NORWAY. Geogr. Ann. Ser. A, Phys. Geogr. 93, 175–191. https://doi.org/10.1111/j.1468-0459.2011.00430.x

Loke, M.H., Dahlin, T., 2002. A comparison of the Gauss–Newton and quasi-Newton methods in resistivity imaging inversion. J. Appl. Geophys. 49, 149–162. https://doi.org/https://doi.org/10.1016/S0926-9851(01)00106-9

Maggi, V., Colucci, R.R., Scoto, F., Giudice, G., Randazzo, L., 2018. Chapter 19 - Ice Caves in Italy, in: Perşoiu,

709 A., Lauritzen, S.-E. (Eds.), Ice Caves. Elsevier, pp. 399–423.
710 https://doi.org/https://doi.org/10.1016/B978-0-12-811739-2.00019-X

711 Maurer, H., Hauck, C., 2007. Instruments and Methods Geophysical imaging of alpine rock glaciers. J.
712 Glaciol. 53, 110–120.

713 Merz, K., Maurer, H., Buchli, T., Horstmeyer, H., Green, A.G., Springman, S.M., 2015. Evaluation of Ground-
714 Based and Helicopter Ground-Penetrating Radar Data Acquired Across an Alpine Rock Glacier.
715 Permafr. Periglac. Process. 26, 13–27. https://doi.org/10.1002/ppp.1836

716 Milan, D.J., Heritage, G.L., Large, A.R.G., Fuller, I.C., 2011. Filtering spatial error from DEMs: Implications for
717 morphological change estimation. Geomorphology 125, 160–171.
718 https://doi.org/https://doi.org/10.1016/j.geomorph.2010.09.012

719 Monnier, S., Camerlynck, C., Rejiba, F., 2008. Ground penetrating radar survey and stratigraphic
720 interpretation of the Plan du Lac rock glaciers, Vanoise Massif, northern French Alps. Permafr.
721 Periglac. Process. 19, 19–30. https://doi.org/10.1002/ppp.610

722 Morard, S., Delaloye, R., Dorthe, J., 2008. Seasonal thermal regime of a mid-latitude ventilated debris
723 accumulation. Proc. 9th Int. Conf. Permafrost, Fairbanks, Alaska 1233–1238.

724 Musil, M., Maurer, H., Green, A.G., Horstmeyer, H., Nitsche, F.O., Mühll, D.V., Springman, S., 2002. Shallow
725 seismic surveying of an Alpine rock glacier. GEOPHYSICS 67, 1701–1710.
726 https://doi.org/10.1190/1.1527071

727 Musil, M., Maurer, H., Hollinger, K., Green, A.G., 2006. Internal structure of an alpine rock glacier based on
728 crosshole georadar traveltimes and amplitudes. Geophys. Prospect. 54, 273–285.
729 https://doi.org/10.1111/j.1365-2478.2006.00534.x

730 Nimis, P.L., Hafellner, J., Roux, C., Clerc, P., Mayrhofer, H., Martellos, S., Bilovitz, P.O., 2018. The lichens of
731 the Alps – an annotated checklist. MycoKeys 31, 1–634. https://doi.org/10.3897/mycokeys.31.23568

732 Oates, J.A.H., 1998. Lime and Limestone: Chemistry and Technology, Production and Uses. WILEY-VCH
733 Verlag GmbH.

734 Oliva, M., Žebre, M., Guglielmin, M., Hughes, P.D., Çiner, A., Vieira, G., Bodin, X., Andrés, N., Colucci, R.R.,
735 García-Hernández, C., Mora, C., Nofre, J., Palacios, D., Pérez-Alberti, A., Ribolini, A., Ruiz-Fernández, J.,
736 Sarıkaya, M.A., Serrano, E., Urdea, P., Valcárcel, M., Woodward, J.C., Yıldırım, C., 2018. Permafrost
737 conditions in the Mediterranean region since the Last Glaciation. Earth-Science Rev. 185, 397–436.
738 https://doi.org/10.1016/j.earscirev.2018.06.018

739 Paterson, W.S.B., 1994. The Physics of Glaciers. Butterworth-Heinemann, Oxford.

740 Pennos, C., Styllas, M., Sotiriadis, Y., Vaxevanopoulos, M., 2018. Chapter 18 - Ice Caves in Greece, in:
741 Perşoiu, A., Lauritzen, S.-E. (Eds.), Ice Caves. Elsevier, pp. 385–397.
742 https://doi.org/https://doi.org/10.1016/B978-0-12-811739-2.00018-8

743 Popescu, R., Vespremeanu-Stroe, A., Onaca, A., Vasile, M., Cruceru, N., Pop, O., 2017. Low-altitude
744 permafrost research in an overcooled talus slope–rock glacier system in the Romanian Carpathians
745 (Detunata Goală, Apuseni Mountains). Geomorphology 295, 840–854.
746 https://doi.org/https://doi.org/10.1016/j.geomorph.2017.07.029

747 Rackl, M., Grötsch, F.E., 2018. 3D scans, angles of repose and bulk densities of 108 bulk material heaps. Sci.
748 Data 5, 180102.

749 Reynolds, J.M., 2011. An Introduction to Applied and Environmental Geophysics, 2nd editio. ed. Wiley-
750 Blackwell.

751 Ribolini, A., Guglielmin, M., Fabre, D., Bodin, X., Marchisio, M., Sartini, S., Spagnolo, M., Schoeneich, P.,

752 2010. The internal structure of rock glaciers and recently deglaciated slopes as revealed by
753 geoelectrical tomography: insights on permafrost and recent glacial evolution in the Central and
754 Western Alps (Italy–France). Quat. Sci. Rev. 29, 507–521.
755 https://doi.org/http://dx.doi.org/10.1016/j.quascirev.2009.10.008

756 Rödder, T., Kneisel, C., 2012. Permafrost mapping using quasi-3D resistivity imaging, Murtèl, Swiss Alps.
757 Near Surf. Geophys. 10, 117–127. https://doi.org/10.3997/1873-0604.2011029

758 Scapozza, C., Mari, S., 2010. Catasto, caratteristiche e dinamica dei rock glaciers delle Alpi ticinesi. Boll.
759 della Soc. Ticin. di Sci. Nat. 98, 15–29.

760 Scotti, R., Brardinoni, F., Alberti, S., Frattini, P., Crosta, G.B., 2013. A regional inventory of rock glaciers and
761 protalus ramparts in the central Italian Alps. Geomorphology 186, 136–149.
762 https://doi.org/10.1016/j.geomorph.2012.12.028

763 Seppi, R., Baroni, C., Carton, A., Bassi, L., 2004. Caratteristiche morfodinamiche di due rock glaciers attivi
764 nel Gruppo Adamello-Presanella. Stud. Trentini di Sci. Nat. Acta Geol. 81, 75–85.

765 Seppi, R., Carton, A., Baroni, C., 2005. Proposta di nuova scheda per il censimento dei rock glaciers da
766 fotografie aeree: applicazione sull'Alta Val d'Ultimo (Gruppo Ortles-Cevedale). Geogr. Fis. e Din. Quat.
767 7, 329–338.

768 Stenni, B., Genoni, L., Flora, O., Guglielmin, M., 2007. An oxygen isotope record from the Foscagno rock-
769 glacier ice core, Upper Valtellina, Italian Central Alps. The Holocene 17, 1033–1039.
770 https://doi.org/10.1177/0959683607082438

771 Thury, M., 1861. Etude Des Glacières Naturelles. Arch. des Sci. la bibliothèque Univers. Genève 1–5.

772 Tretiach, M., 1992. Lichenological studies in NE-Italy. V: new records from Friuli-Venezia Giulia. Stud.
773 Geobot. 12, 3–60.

774 Vieira, G., Mora, C., Faleh, A., 2017. New observations indicate the possible presence of permafrost in
775 North Africa (Djebel Toubkal, High Atlas, Morocco). Cryosph. 11, 1691–1705.
776 https://doi.org/10.5194/tc-11-1691-2017

777 Wahrhaftig, C., Cox, A., 1959. Rock glaciers in the Alaska Range. Bull. Geol. Soc. Am. 70, 383–436.
778 https://doi.org/10.1130/0016-7606(1959)70[383:RGITAR]2.0.CO;2

779 Whalley, W.B., Martin, H.E., 1992. Rock glaciers : II models and mechanisms. Prog. Phys. Geogr. 16, 127–
780 186. https://doi.org/10.1177/030913339201600201

781 Wheaton, J.M., Brasington, J., Darby, S.E., Sear, D.A., 2010. Accounting for uncertainty in DTMs from repeat
782 topographic surveys: improved sediment budgets. Earth Surf. Process. Landforms 35, 136–156.

783 Zhang, Z., 1994. Iterative point matching for registration of free-form curves and surfaces. Int. J. Comput.
784 Vis. 13, 119–152. https://doi.org/10.1007/BF01427149

785